An Investigation of the Ability of Nonlinear Methods to Infer Dynamics from Observables

A. A. Tsonis,*
G. N. Triantafyllou,*
J. B. Elsner,+
J. J. Holdzkom II,**
and A. D. Kirwan Jr.**

Abstract

In this study analysis of data whose character was kept secret was performed by employing a variety of nonlinear approaches. The idea was to test the ability of approaches stemming from the theory of nonlinear dynamical systems to infer the true properties hidden in the data. The approaches employed include dimension estimation, nonlinear prediction, Lyapunov exponent estimation, and false nearest neighbors. It is concluded that even though the methods have problems and occasionally may be inconclusive, when correctly applied they are effective in delineating the dynamics underlying the data.

1. Introduction

In the XVIII General Assembly of the European Geophysical Society (EGS) in Weisbaden, Germany, 3–7 May 1993, a session dealt with nonlinear time series analysis and prediction in geophysical fluid dynamics. Among the papers presented were several studies dealing with the estimation of properties of reconstructed attractors from observables. In the ensuing discussions, questions were raised regarding the effectiveness of "black boxes" (algorithms) when they are used blindly, as, for example, with an observable from an *unknown* system. The algorithms have been developed by testing them with observables from a priori known systems. Does this make them always applicable? How efficiently do they perform when they are faced with time series from an unknown (to the investigator) time series? As a result of this interesting discussion ADK challenged the audience with the following simple proposition: If I provide synthetic time series and only I know how they are generated, can you examine them and tell me what they are? The challenge was accepted by AAT, GNT, and JBE. ADK and JJH supplied us with 10 synthetic time series from models known only to them. One hundred thousand equally spaced in time values for each time series were supplied. From these 10 time series, 4 were chosen at random and analyzed. This paper reports on the approaches used to identify the properties of the models, followed by the presentation of the models by ADK and JJH. In the following section it is assumed that the concepts and method behind the employed methods are known and extensive repetition of what can be found in many books and papers (e.g., Tsonis 1992, and references herein) is avoided. The theme of this contribution is the extraction of information from data. Thus, it is similar to the Santa Fe contest on prediction of several time series that emerged out of informal discussions at the Complex Systems Summer School at the Santa Fe Institute in the summer of 1990 (Gershenfeld and Weigend 1993). The difference is that the purpose of the analyses here is not to investigate predictability but to assess the ability of several approaches to investigate the dynamics that underlie the observables. Thus, only data whose dynamics can be linked to available models could be worked with.

2. Data analysis and results

a. Time series 1

Figure 1a shows the first of the four time series investigated here. As a first step two products from conventional linear time series analysis are presented, namely, the autocorrelation function and power spectra (Figs. 1b and 1c, respectively). The autocorrelation function seems to be periodic but somewhat complicated. The spectra show peaks, some of which can be identified as combinations of two frequencies. No significant background (broadband) noise is evident.

From Fig. 1 an argument could then be made that what is shown is some kind of a quasi-periodic signal. If the corresponding attractor is some torus, it should be possible to obtain from nonlinear methods a corre-

*Department of Geosciences, University of Wisconsin—Milwaukee, Milwaukee, Wisconsin.
+Department of Meteorology, The Florida State University, Tallahassee, Florida.
**Center for Coastal Physical Oceanography, Old Dominion University, Norfolk, Virginia.
Corresponding author address: A. A. Tsonis, Department of Geosciences, University of Wisconsin—Milwaukee, Lapham Hall, P. O. Box 413, Milwaukee, WI 53201.
In final form 21 April 1994.

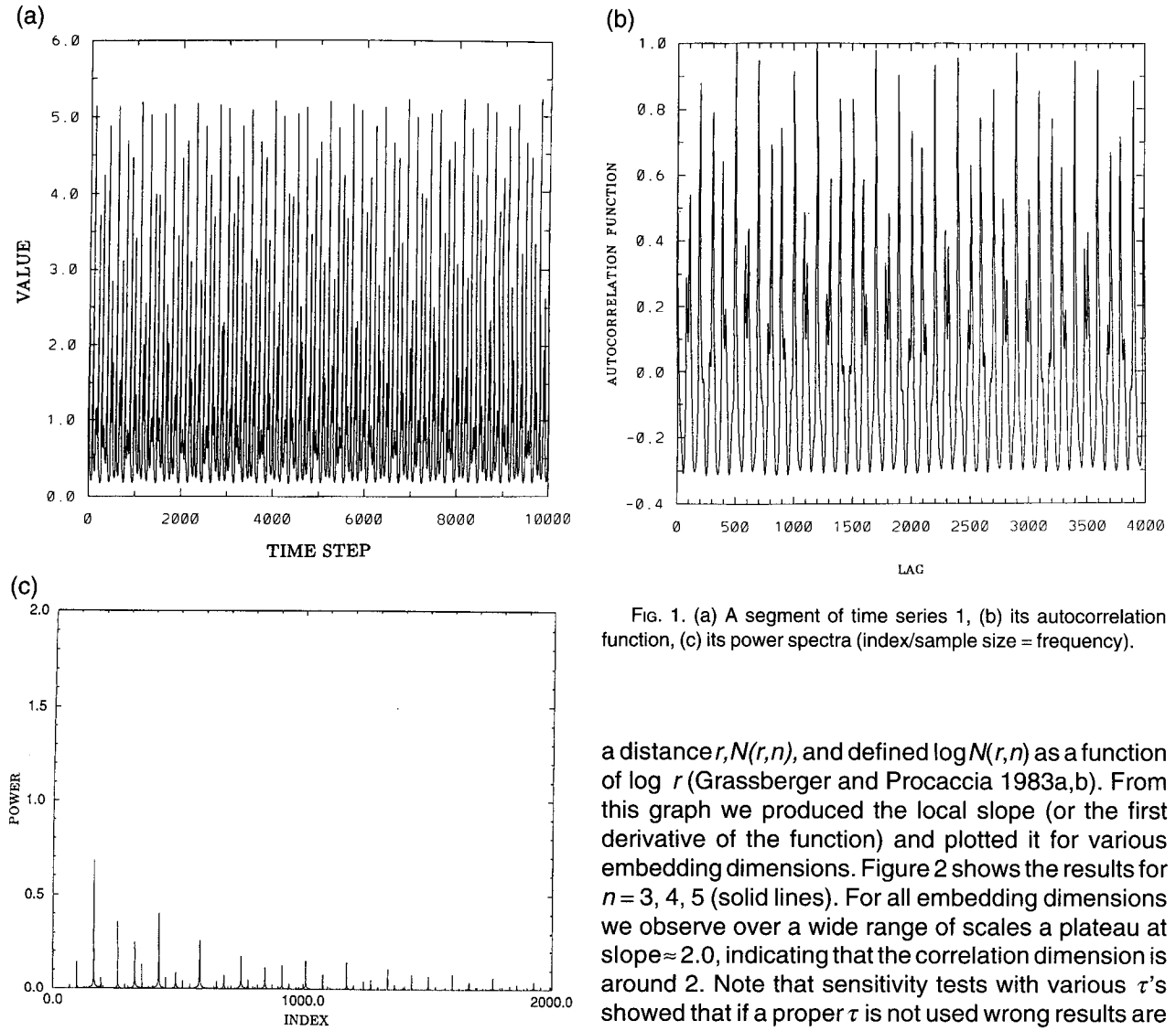

FIG. 1. (a) A segment of time series 1, (b) its autocorrelation function, (c) its power spectra (index/sample size = frequency).

lation dimension of 2, a proper embedding of 3, no positive Lyapunov exponents, and a nonlinear prediction where the skill oscillates as a function of the time step.

1) CORRELATION DIMENSION

From Fig. 1b it is observed that for a lag equal to 75 the autocorrelation function is approximately zero. We thus considered a delay parameter $\tau = 75$ and constructed the vector

$$\mathbf{X}(t_i) = \{\mathbf{x}(t_i), \mathbf{x}(t_i + \tau), \ldots, \mathbf{x}[t_i + (n-1)\tau]\},$$

where n represents the embedding dimension and $\mathbf{x}(t_i)$ is the first 45 000 values of our time series. Note that this way to determine τ, even though it is widely used, is not universally accepted. Other methods are also available (see Tsonis 1992). We then estimated the number of pairs of points that are separated by at least a distance r, $N(r,n)$, and defined $\log N(r,n)$ as a function of $\log r$ (Grassberger and Procaccia 1983a,b). From this graph we produced the local slope (or the first derivative of the function) and plotted it for various embedding dimensions. Figure 2 shows the results for $n = 3, 4, 5$ (solid lines). For all embedding dimensions we observe over a wide range of scales a plateau at slope ≈ 2.0, indicating that the correlation dimension is around 2. Note that sensitivity tests with various τ's showed that if a proper τ is not used wrong results are obtained. For example, when $\tau = 500$ is used a different attractor is delineated and a correlation dimension equal to 1.6 is estimated (dotted lines in Fig. 2). This is an important result since it points out that when dealing with data exhibiting oscillating autocorrelation functions the choice of τ is critical. An indication of chaotic dynamic may be suggested if the wrong τ is used! Phase-space reconstruction in 3D further demonstrates this point (Fig. 3). When $\tau = 500$ is used (Fig. 3a) a different structure is obtained than when $\tau = 75$ is used (Fig. 3b).

An independent way to infer dimensions has recently been proposed by Abarbanel and Kennel (1992) and Sugihara and May (1990). The first method is based on the nearest neighbors and its basic philosophy is outlined in Fig. 4. If the underlying attractor is assumed to be a circle and the motion is embedded in one dimension then points close to 1 and 3 will be closer neighbors. We call these neighbors false neighbors because in the actual motion they are very far apart. Thus, starting with $d = 1$ for each point in phase

space we find the nearest neighbor. From all the available points we then find how many of those nearest neighbors remain nearest neighbors as we go to $d=2$, $d=3$, and so on. The embedding for which the percentage of false neighbors goes to zero provides, according to Abarbanel and Kennel, an integer-valued dimension of the underlying dynamics, especially if the noise in the data is small. Figure 5 shows the results for $\tau=75$ when this approach is applied to time series 1. At embedding dimension 3 the ratio is almost zero and remains as such for higher embeddings. This indicates that the actual motion takes place on an attractor embedded in three dimensions. Since a 2-torus must be embedded in three dimensions this result is compatible with the correlation dimension estimate for time series 1. The other approach is based on nonlinear prediction and it will be discussed in a later section.

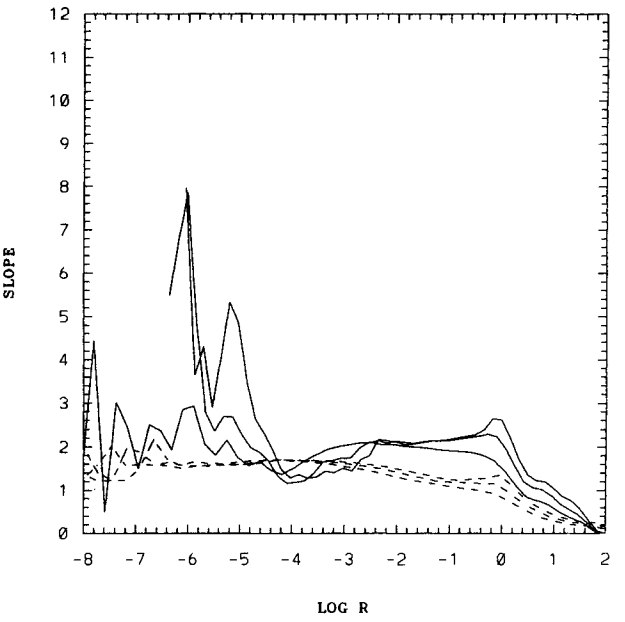

FIG. 2. Slope as a function of log$r$ for time series 1 for embedding dimensions 3, 4, and 5 (solid lines). Results based on $\tau=75$, which corresponds to a zero in the autocorrelation function. A plateau around a value of slope ≈ 2 is observed. The dotted lines show the same but for $\tau=500$, which corresponds to a highly autocorrelated value. Now the plateau is observed at a lower level (≈ 1.6).

2) LYAPUNOV EXPONENTS

The Lyapunov exponents provide the rate at which nearby trajectories diverge or converge as they evolve according to the underlying dynamics. There are as many Lyapunov exponents as coordinates of the embedding space. Periodic systems have one, two, three, or more (depending on whether or not the motion is described by a limit cycle, a 2-torus, a 3-torus, or some higher dimensional torus, respectively) Lyapunov exponents that are zero, with the rest being negative. Chaotic systems have at least one positive Lyapunov exponent indicating the property of divergence of nearby trajectories. We estimated the Lyapunov exponents of time series 1 using again the first 45 000 points and the algorithm proposed by Eckman et al. (1986) and obtained $\lambda_1 = 0.07$,

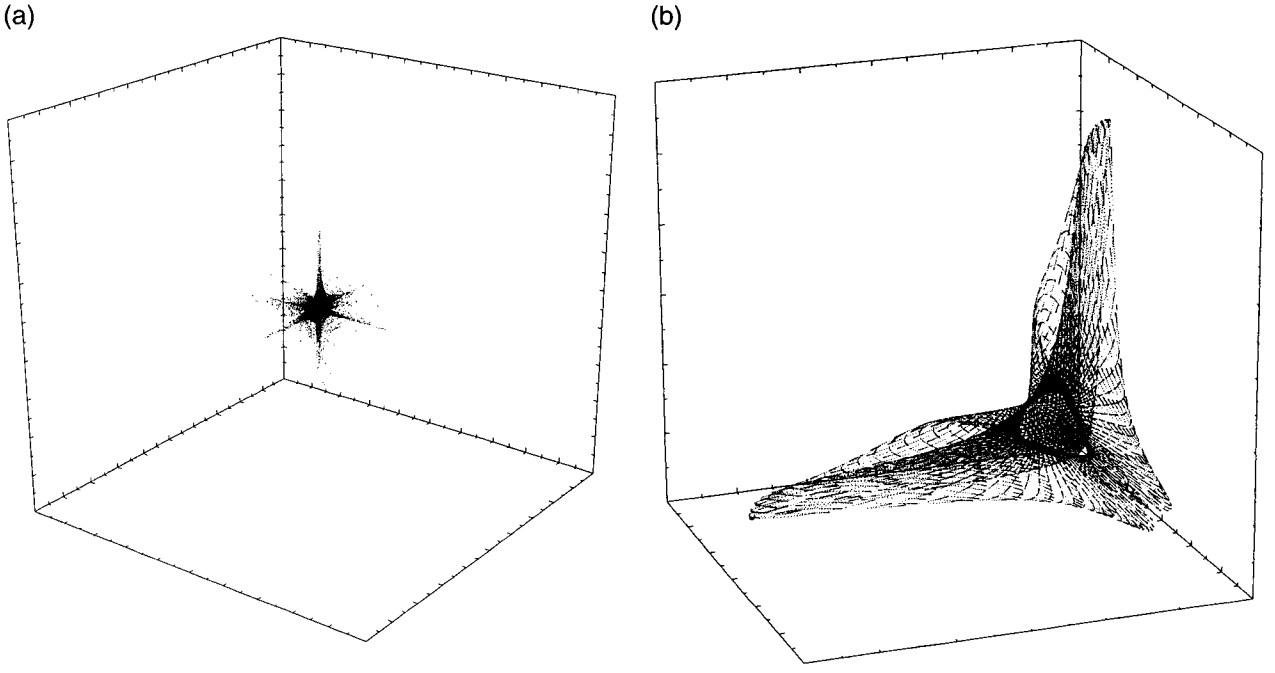

FIG. 3. (a) Three-dimensional phase-space reconstruction for $\tau=500$; (b) 3D phase-space reconstruction for $\tau=75$.

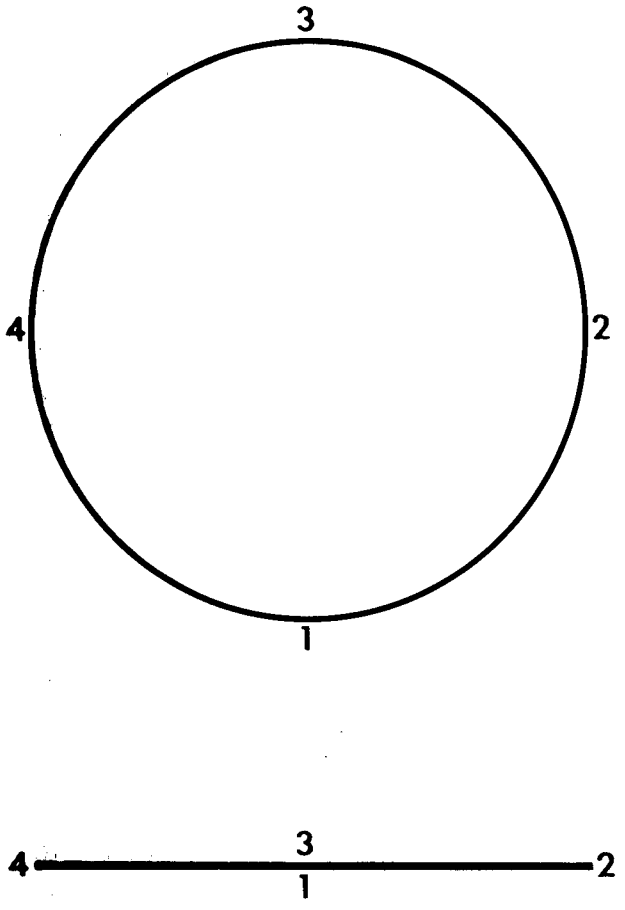

FIG. 4. An illustration of the principle behind estimating the embedding dimension using nearest neighbors (see text for details).

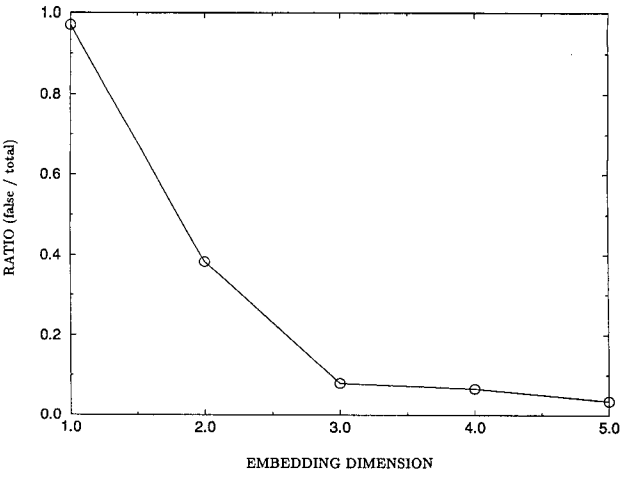

FIG. 5. Ratio of false neighbors to the total neighbors for time series 1 as a function of the embedding dimension. From this figure we can estimate that an integer-valued dimension for the underlying dynamics is equal to 3 (in other words, the motion takes place on an attractor embedded in three dimensions).

$\lambda_2 = -0.009$, $\lambda_3 = -0.11$, and $\lambda_1 = -0.34$. The first two Lyapunov exponents are close to zero and could be interpreted as indicating a motion on a torus. We feel, however, that λ_1 is somewhat high. Chaotic dynamical systems whose dimension is just above 2 (e.g., the Rossler system) exhibit a positive Lyapunov exponent around 0.13. It may, therefore, be that a value of 0.07 is within the error bounds of a torus. We do feel, however, a little apprehensive in attributing these results to either a torus or to some very mild chaotic motion.

3) NONLINEAR PREDICTION

If an underlying deterministic mechanism exists, then the order with which the points appear in the attractor will also be deterministic. Thus, if it is possible to extract the rules that determine where the next point will be located in phase space a very accurate prediction will be obtained. In general, in nonlinear predictions it is assumed that the underlying dynamics can be written as a map of the form

$$x(t + T) = f_T[x(t)],$$

where in phase space $x(t)$ is the current state and $x(t + T)$ is the state after some time interval T.

Since the form of the attractor is not known a priori one approach is to estimate the above mapping locally (Farmer and Sidorowich 1987). This so-called local approximation takes a point $x(t)$ of the attractor reconstructed at some proper embedded space and considers around it a small neighborhood containing points generated in the past. By comparing the motion of the neighbors after a time step T one can construct a mapping that dictates the motion of the neighborhood and thus of point $x(t)$. The form of f can be anything, but the simplest way is to consider it linear and construct the mapping every time step into the future. Note that since the linear mapping may not be the same for each time step the overall procedure is *not* linear. If a system is chaotic one expects that predictability will deteriorate with time, and thus one should expect that the correlation $r(t)$ between actual and predicted values as function of prediction time exhibits a "falloff." Such falloff would not be expected if the signal is periodic [$r(t)$ is equal to one and independent of t]. Additive noise superimposed over a periodic signal will offset the above level by a constant amount, and if the signal is quasi-periodic $r(t)$ will oscillate with t (Sugihara and May 1990; Tsonis 1992; Elsner and Tsonis 1992; Sugihara 1993, personal communication).

According to Sugihara and May (1990), nonlinear prediction can by itself provide a way to determine a proper embedding for the data. The idea is that once a proper embedding has been found, the correlation coefficient between actual and predicted values, $r(t)$,

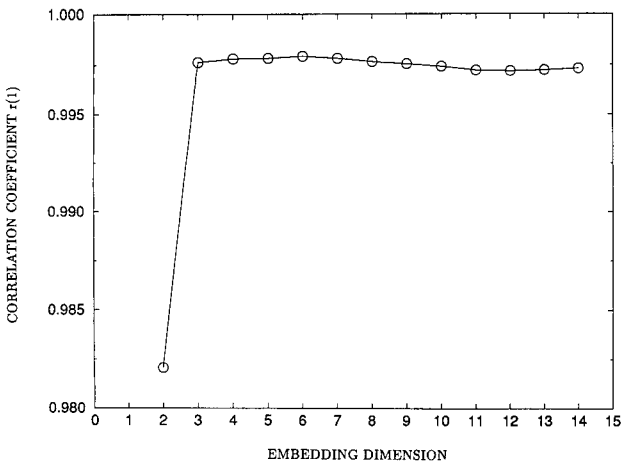

FIG. 6. Correlation coefficient between actual and predicted value for one-step prediction [$r(1)$] for time series 1 as a function of the embedding dimension. The correlation increases and levels off at an embedding dimension 3, which indicates that this is a proper embedding dimension.

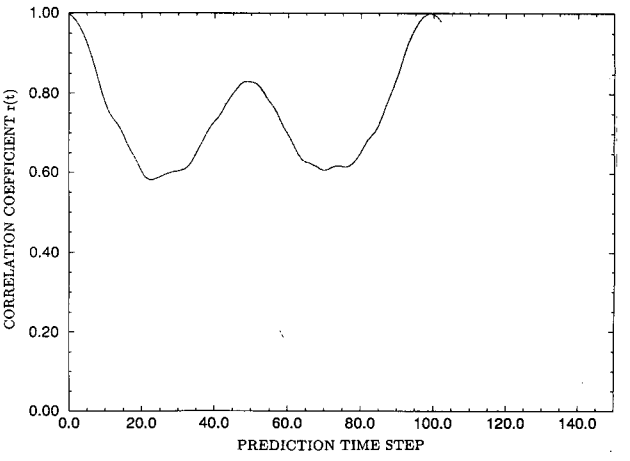

FIG. 7. Correlation coefficient $r(t)$ between actual and predicted values for time series 1 as a function of prediction step. The skill oscillates, indicating a quasi-periodic motion.

should not change. In other words predictability will increase as correct embedding is approached, and after that the result will remain the same. Figure 6 shows $r(1)$ [i.e., $r(t)$ for the first time step prediction] as a function of the embedding dimension for time series 1 and $\tau = 75$. As can be seen $r(1)$ levels off and stays at a level of about 0.9975 for embedding dimension 3 and higher. This result supports the results reported in section 2a(1) indicating that the motion is taking place in an attractor embedded in three dimensions.

Figure 7 shows $r(t)$ as a function of t for embedding dimension 3 and $\tau = 75$. Here the first 10 000 points are used for training (i.e., to derive the linear mapping) and the next 10 000 are used for testing. Thus, $r(t)$ values are based on a sample size of 10 000. The correlation between actual and predicted value oscillates at a constant level as the prediction time increases indicating, as mentioned above, a motion on a torus (quasi-periodic motion).

In summary, correlation dimension estimates, false nearest neighbors, and nonlinear prediction suggest a quasi-periodic motion on a 2-torus. Even though the Lyapunov exponents are not as conclusive as the other tests, our decision is that time series 1 represents a quasi-periodic signal.

b. Time series 2

Figure 8 shows time series 2. Exactly the same tests were applied here as well, and the results are summarized in Table 1. All tests except for the nearest neighbors test indicate a quasi-periodic motion. Here the first two Lyapunov exponents are very close to zero and at least an order of magnitude smaller than the rest. We therefore will consider them as equal to zero. Thus, having four conclusive and one inconclusive tests, our verdict is that again we are dealing with an observable from a quasi-periodic system.

TABLE 1. Summary of the results for time series 2.

Autocorrelation function	**Spectra**	**Correlation dimension**	**Nearest neighbors**	**Lyapunov exponents**	***r*(1) vs d_e**	***r*(*t*) vs *t***
Decorrelation time $\tau = 50$	Several pronounced peaks attributed to combinations of two major frequencies	Estimated to be two over a range of scales at least 5 decades wide	Inconclusive	$\lambda_1 = 0.009$ $\lambda_2 = -0.003$ $\lambda_3 = -0.21$ $\lambda_4 = -0.95$ $\lambda_5 = -8.3$	Leveling off at $d_e = 3$	Oscillating in time at a constant level

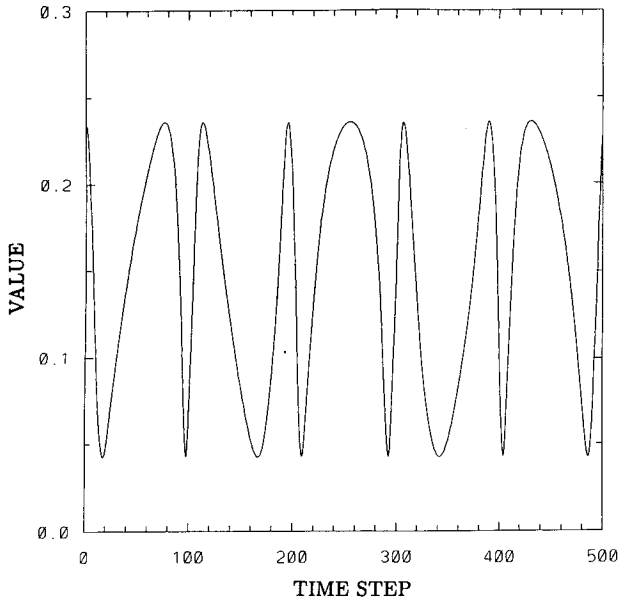

FIG. 8. A sample of time series 2.

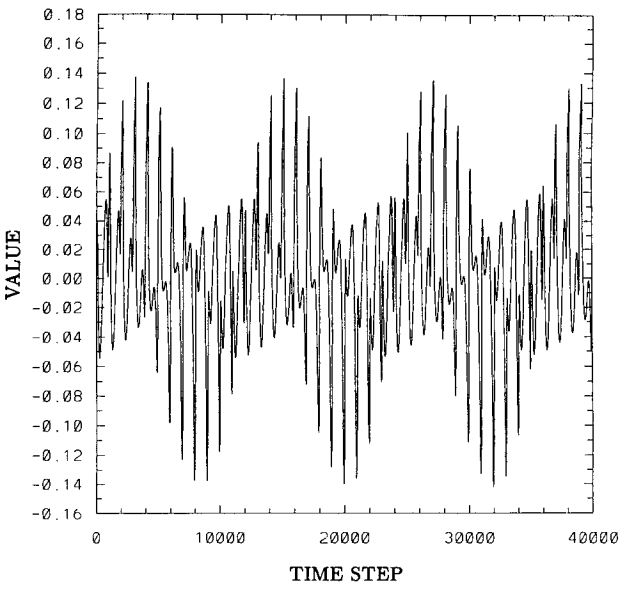

FIG. 9. A sample of time series 3.

c. Time series 3

Figure 9 shows the time series and Table 2 summarizes the results. Here, three tests suggest a 2-torus and two tests [$r(1)$ versus d_e and possibly the Lyapunov exponents] are inconclusive. We again decide in favor of a quasi-periodic motion.

We wish to stress here a point very much related to the philosophy of this paper. The reported Lyapunov exponents were in two cases inconclusive. In those cases the first two exponents are very close to zero and it may be that in fact they are within the error bounds of the algorithm for a quasi-periodic motion. This is, however, something that a given algorithm (or "black box") cannot resolve. Other algorithms may perform more satisfactorily, but the bottom line is that a blind application of an algorithm may not always be conclusive.

d. Time series 4

Figure 10 shows time series 4. Visual examination of this figure indicates that the statistical properties of this signal do not remain the same in time. Intermittency and oscillation "packets" whose amplitude increases with time are observed. We considered the three different parts of the signal where it looks like the statistical properties may remain constant, namely the segment from 1–30 000, the segment from 30 000–55 000, and the segment from 65 000–90 000, and estimated their autocorrelation functions (Fig. 11). Apparently, the autocorrelation structure in the three time segments is vastly different. In fact we believe that even within the chosen segments the statistical properties do not remain the same. For example, in Fig. 10 and for the first segment an apparent increase of the amplitude of the oscillation can be observed.

TABLE 2. Summary of the results for time series 3.

Autocorrelation function	Spectra	Correlation dimension	Nearest neighbors	Lyapunov exponents	$r(1)$ vs d_e	$r(t)$ vs t
Decorrelation time $\tau = 200$	Several pronounced peaks attributed to combinations of two major frequencies	Estimated equal to two over a range of scales at least 5 decades wide	Indicating an embedding of three	$\lambda_1 = 0.08$ $\lambda_2 = -0.003$ $\lambda_3 = -0.39$ $\lambda_4 = -0.17$ $\lambda_5 = -10.1$	Inconclusive	Oscillating in time at a constant level

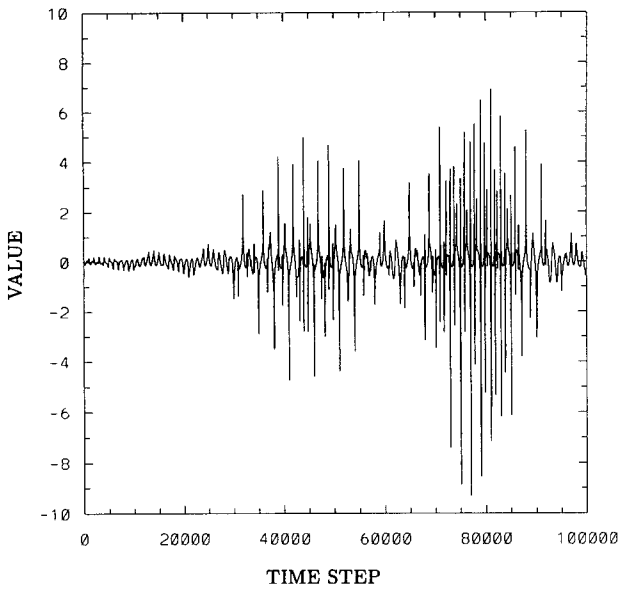

FIG. 10. Time series 4 in its entirety. Here, one can distinguish three different segments where the statistical properties differ. Those are approximately the part from 1–30 000, the part from 30 000–55 000, and the part from 65 000–90 000 time steps.

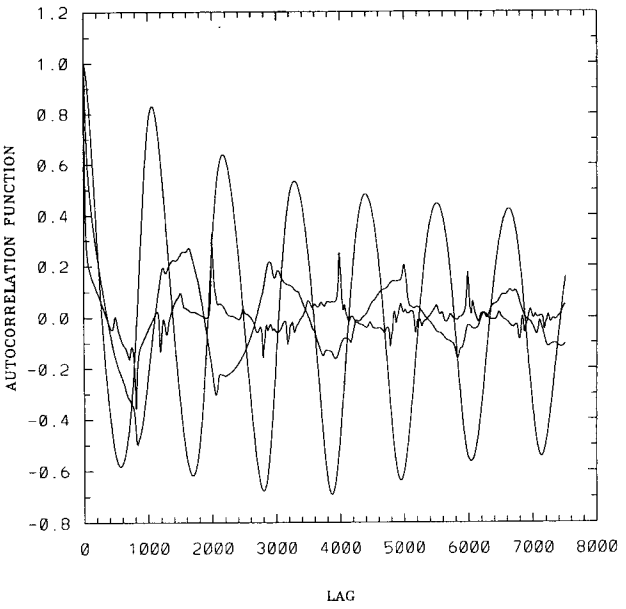

FIG. 11. Autocorrelation function for the three distinct parts of time series 4. Each segment exhibits different autocorrelation structure, indicating the absence of a "fixed" dynamic throughout.

Similar comments can be made for the other two segments. Figure 12 shows the local slope as a function of log r for embedding dimensions 3, 4, and 5 for the entire sequence. Notice the absence of scaling. These functions are rather nonlinear, exhibiting no plateau. It is interesting, however, to notice that the functions remain virtually unchanged as the embedding dimension increases and they are confined at low slope values (below 3). That prompted us to investigate the properties of a reconstruction in three dimensions. Figures 13a and 13b show such a reconstruction based on the first 50 000 points and on the whole time series (100 000 points), respectively. We clearly see the structure of the attractor as being something like a three-dimensional star. The geometry of the structure does not change as we increase the number of points; the structure simply grows bigger. Given the nature of our signal this geometry can be completely explained. Due to the intermittent character of the time series most of the values are found around zero. Those values result in the center "black" sphere shown in Fig. 13. The intermittency bursts manifest themselves as points away from that sphere. Note, however, that there is some structure in those bursts since the corresponding points are found along certain directions only. The fact that the structure grows as more points are included indicates that the provided signal, even though very long, does not represent a full "orbit." Consequently, we can explain the function observed in Fig. 12. The domination of the points around zero biases the dimension at smaller scales toward small values. At longer scales the algorithm begins to see the three-dimensional structure and thus the dimension approaches a value of 3.

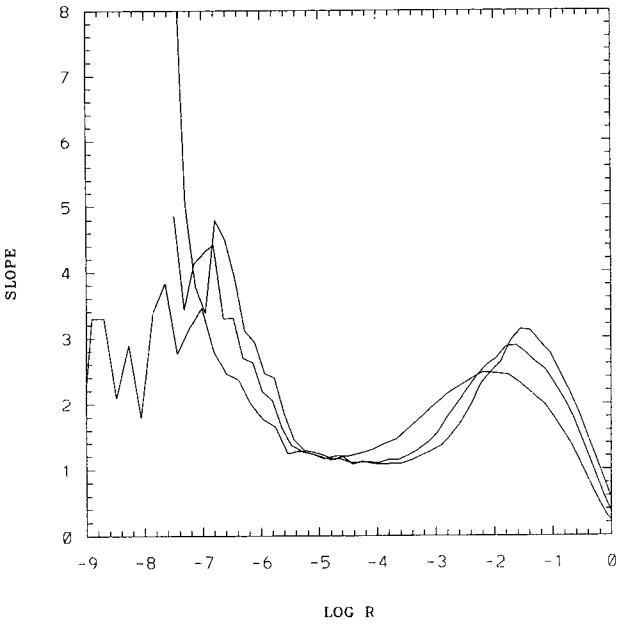

FIG. 12. Slope as function of log r for time series 4 for embedding dimensions 3, 4, and 5. Based on $\tau = 352$, which corresponds to a zero in an autocorrelation function of the entire series. Note the absence of a plateau.

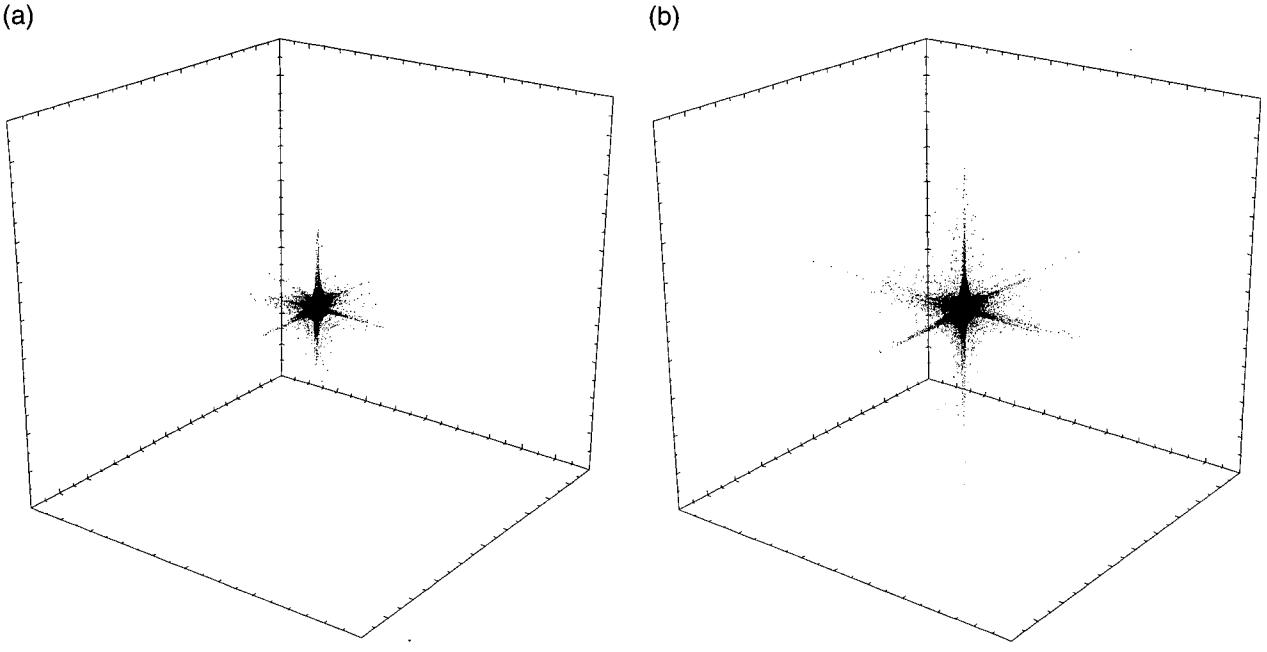

FIG. 13. Three-dimensional phase-space reconstruction from (a) the first 50 000 points of time series 4 and (b) the entire sample.

The actual dimension is between 2 and 3, but an accurate estimation of the dimension requires many more points. Lyapunov exponents estimation, nonlinear prediction, etc., also produce similar conclusions. Thus, provided that this solution is stable (i.e., the oscillation "packets" will not keep increasing in amplitude forever), we have to conclude that the signal in question does not even represent a full "orbit"! In this case the signal might be chaotic since the autocorrelation structure in the various segments shows a steady amplitude decrease with lag, indicating loss in memory, and the corresponding spectra (not shown) exhibit significant broadband structure.

3. The dynamic model

The time series analyzed above were produced by a fully nonlinear two-layer inviscid hydrodynamic model in a rotating frame, often called an f plane. The upper layer is confined to a parabolic ellipsoid, whereas the bottom layer is infinite in the horizontal direction. The appropriate nondimensional, vertically integrated hydrodynamic equations are well known to be

$$\frac{D}{Dt}U_i^{(1)} + \sigma_{ij}U_j^{(1)} + \frac{\partial\left[h^{(1)}+h^{(2)}\right]}{\partial x_i} = 0 \qquad (1)$$

$$\frac{D}{Dt}h^{(1)} + h^{(1)}\frac{\partial U_j^{(1)}}{dx_j} = 0 \qquad (2)$$

$$\frac{D}{Dt}U_i^{(2)} + \sigma_{ij}U_j^{(2)} + \frac{\partial}{\partial x_i}\left[(1-\varepsilon_{21})h^{(1)} + h^{(2)}\right] = 0 \qquad (3)$$

$$\frac{D}{Dt}h^{(2)} + h^{(2)}\frac{\partial U_j^{(2)}}{\partial x_j} = 0. \qquad (4)$$

Here, $U_i^{(\alpha)}$ is the ith velocity component in the α layer and $h^{(\alpha)}$ is the $\alpha = 1, 2$ layer thickness. Also, $D/Dt = \partial/\partial t + U_j\partial/\partial x_j$ is the material derivative;

$$\sigma_{ij} = \begin{bmatrix} 0 & -1 \\ 1 & 0 \end{bmatrix}$$

is the rotation matrix; and $\varepsilon_{21} = (\rho_2 - \rho_1)/\rho_2$ is the density contrast between the layers. In all, Eqs. (1)–(4) represent six nonlinear coupled partial differential equations. These equations can be dimensionalized using

$$h^* = H^* h$$
$$x_i^* = x_i(g^* H^*/f^{*2})^{1/2}$$
$$t^* = t/f^*.$$

Here, $(\ )^*$ quantities are dimensional, f^* is the Coriolis parameter, g^* is the reduced gravity, and H^* is the upper-layer vortex-scale thickness.

General solutions to Eqs. (1)–(4) must be obtained numerically. Standard numerical recipes such as finite differences cannot recover the full range of nonlinear

behavior without paying an enormous computational penalty. Fortunately there is an alternate approach that does fully account for the nonlinearity and is in keeping with the spirit of dynamical systems. The first step in implementing the approach is to focus on the response of the confined upper layer when flow in the lower layer is prescribed.

Following Ruddick (1987), lower-layer pressure fluctuations are expressed in terms of the prescribed lower-layer velocity, and, after the superscripts for layer 1 are dropped, Eqs. (1)–(4) reduce to

$$\frac{D}{Dt}U_i + \sigma_{ij}U_j + \frac{\partial}{\partial x_i}h = L_i, \tag{5}$$

$$\frac{D}{Dt}h + h\frac{\partial U_j}{\partial x_j} = 0, \tag{6}$$

where $L_i = DU_i^{(2)}/Dt + \sigma_{ij}U_j^{(2)}$.

The next step is to use a low-order spectral expansion for the field variables in the upper layer. Following Cushman-Roisin et al. (1985), solutions are sought on the form

$$U_1 = (G/2 + G_N)x_1 + (G_S - G_R)x_2 \tag{7}$$

$$U_2 = (G_S + G_R)x_1 + (G/2 - G_N)x_2 \tag{8}$$

$$h = h_0 + (B/2 + B_N)x_1^2 + 2B_S x_1 x_2 + (B/2 - B_N)x_2^2. \tag{9}$$

Equations (7)–(9) are valid only for $h \geq 0$, since the vortex is confined to this region. Here, h_0 is the centerline thickness of the upper layer. Also, G and G_R are the divergence and spin of the vortex velocity field, while G_N and G_S are the shear and normal deformation rates. The surface boundary signature of the vortex is determined by h_0, B, B_N, and B_S. As shown by Kirwan and Liu (1991), the semimajor and semiminor axes of the vortex are given, respectively, by

$$R_a = h_0\left[|B/2| - \left(B_N^2 + B_S^2\right)^{1/2}\right]^{-1/2}$$

$$R_b = h_0\left[|B/2| + \left(B_N^2 + B_S^2\right)^{1/2}\right]^{-1/2}.$$

Also, the ellipse and velocity vector orientations are given, respectively, by

$$\alpha = (1/2)\tan^{-1}(B_S/B_N)$$

$$\beta = (1/2)\tan^{-1}(-G_N/G_S).$$

A dynamical system of eight coupled, nonlinear ordinary differential equations is obtained when Eqs. (7)–(9) are substituted into (5) and (6). These are

$$dh_o/dt + h_oG = 0 \tag{10}$$

$$dB/dt + 2[BG + 2(B_NG_N + B_SG_S)] = 0 \tag{11}$$

$$dB_S/dt + 2B_SG + G_SB - 2B_NG_R = 0 \tag{12}$$

$$dB_N/dt + 2B_NG + G_NB + 2B_SG_R = 0 \tag{13}$$

$$dG/dt + G^2/2 + 2(G_N^2 + G_S^2 - G_R^2 - G_R + B) = L_G \tag{14}$$

$$dG_R/dt + GG_R + G/2 = 0 \tag{15}$$

$$dG_N/dt + GG_N - G_S + 2B_N = L_N \tag{16}$$

$$dG_S/dt + GG_S + G_N + 2B_S = L_S. \tag{17}$$

Here, L_i is expressed in terms of its spherical, deviator, and skew components (Eringen 1962), and

$$L_G = dG^{(2)}/dt + (G^{(2)})^2/2 + 2[(G_N^{(2)})^2 + (G_S^{(2)})^2 - (G_R^{(2)})^2 - G_R^{(2)}] \tag{18}$$

$$L_N = dG_N^{(2)}/dt + G^{(2)}G_N^{(2)} - G_S^{(2)} \tag{19}$$

$$L_S = dG_S^{(2)}/dt + G^{(2)}G_S^{(2)} - G_N^{(2)}. \tag{20}$$

Solutions to Eqs. (10)–(17) were obtained using a double precision, fifth-order Runge–Kutta solver that adjusts the time step size to meet a tolerance of 10^{-9}. All of the solutions presented here are numerically stable.

The unforced equations ($L_G = L_N = L_S = 0$) have five known invariants (Ball 1963). These are related to conservation of eddy (hereafter referred to as lens) volume, potential vorticity, angular momentum, total energy, and potential deformation (Kirwan and Liu 1991). Thus, the number of dynamically independent variables is three for this case. Although this unforced canonical system is nonlinear, it is not believed to have chaotic solutions. However, for appropriate initial conditions the solutions can be quite complicated. With the forcing prescribed above, only the volume and potential vorticity invariants remain, so that the number of dynamically independent variables for such cases is six. As reported by Kirwan et al. (1992) and Kirwan and Lipphardt (1993), solutions to the forced system exhibit some chaotic properties. However, a complementary analysis from the standpoint of dynamical systems theory has not yet been made.

TABLE 3. Initial conditions for lenses 1 and 2. Here X_0 and Y_0 are the initial locations of a particle. The other symbols are explained in text.

Case	h_0	B	B_S	B_N	G	G_R	G_N	G_S	X_0	Y_0
Lens 1	1.0	−0.223607	0.0	−0.01	0.0	−0.238972	0.0	−0.978907	0.0	9.20442
Lens 2	1.0	−0.223607	0.0	−0.01	0.0	−1.492297	0.0	−0.20431	0.0	9.20442

Prior experience with this model has shown that it can exhibit a very wide spectrum of behavior. This includes analytic solutions for special initial conditions to ragged and spikey time series for the variables. The spikey character can result from the fact that some variables spend more time during an oscillation cycle close to some preferred value and just a brief interval at an extreme value. Then standard statistical methods give averages that are very close to the preferred value since many more of these are contained in the average than in the extreme values. Also, the standard deviation does not represent the biased character of the scatter about the mean. The spikey character can also frustrate spectral analysis. Even if only one frequency is present, the spectral routine may require many spectral amplitudes to resolve the time series.

Three test time series groups were prepared and transmitted to the analysts. Initial conditions for these simulations are given in Table 3. Lenses 1 and 2 were unforced cases; that is, $L_i = 0$ in Eqs. (10)–(17). Presumably these are nonchaotic cases. Lens 3 was a forced case. The initial conditions were the same as lens 2; however, the forcing was prescribed as the solution for lens 2—that is, this system was resonately forced. For a linear system this would produce secular growth in the time series. However, for this system the nonlinearity actually stabilizes the solution. Of course, if the amplitudes of the forcing are large enough the solutions will evolve (but not always quickly) to a lens infinitely thin but of infinite radius. In addition, since the system is forced by lens 2, which exhibits low-frequency oscillations, its solutions might also be exhibiting very low frequency oscillations. See discussion in Kirwan et al. (1992) for further details.

Table 4 shows the time series that were transmitted to the analysts. Several points should be made concerning this. First, not all of the dynamical variables were made available. For lens 1 the only dynamical variable was h_o, and as can be seen from Eq. (10) it is coupled only to the G field (horizontal divergence); this is a one-way coupling. Also, for lens 1 the particle path data is merely a mapping and R_b/R_a is derived from the B-field time series. For lenses 2 and 3 the deformations G_N and G_S were supplied along with path data.

The analysts chose to analyze lens 1 column 2 (time series 1), lens 1 column 5 (time series 2), lens 2 column 2 (time series 3), and lens 3 column 2 (time series 4). It is clear that they correctly deduced the essential dynamics for lenses 1 and 2 even with limited time series and no a priori knowledge of the physics. This was accomplished with the new techniques of dynamical systems theory. As discussed above, classical statistical/spectral methods may not be decisive for these two cases.

The description of lens 3 is essentially correct as well. As mentioned above, the solution is stable. Thus the solution will not blow up. It exhibits, however, very low frequency oscillations, which results in nonstationary segments (like those supplied to the analysts). In fact, those oscillations might have periodicities in excess of 5×10^5 data points. Because of that, exact estimation of the Lyapunov exponent spectrum from

TABLE 4. Time series supplied to analysts. The correspondence with the time series employed by the analysts is as follows: time series 1: lens 1 col 2; time series 2: lens 1 col 5; time series 3: lens 2 col 2; time series 4: lens 3 col 2. Here, $\gamma = G_N^2 + G_S^2 - G_R^2$.

Case	Col 1	Col 2	Col 3	Col 4	Col 5	Col 6	Time	Step
Lens 1	T	h_0	X	Y	R_b/R_a	γ	0–1000	0.01
Lens 2	T	G_N	G_S	X	Y		0–100	0.001
Lens 3	T	G_N	G_S	X	Y		0–100	0.001

the equations is not feasible given the computational effort involved. Solutions are sensitive to initial conditions and parameter values that are characteristic for chaotic behavior (Kirwan and Lipphart 1993; Kirwan et al. 1992). Thus, it is again clear that the algorithms were able even with limited data to point out useful properties of the system.

4. Summary

An assessment of the ability of nonlinear methods to infer dynamics from observables was attempted here. One group (ADK and JJH) supplied time series whose dynamics were known to them only and the rest of us attempted to extract as much information as possible. From this combined effort we conclude that nonlinear approaches stemming from the theory of chaos can provide useful information about the underlying dynamical system. Preferably, not just one but all possible approaches should be considered and the results should be compared collectively. However, due to the inherent problems and weaknesses of the involved algorithms it is imperative that they are applied properly; otherwise, wrong conclusions can be reached. Most of the generated series (lens 1 and lens 2) were nonchaotic. Such a design explores uniformly the range of dynamics of the model and reflects our initial concern not to overwhelm the analysis with chaotic time series (the type of data on which all those methods were developed), but also to test the methods in cases of strong nonlinearity not necessarily associated with chaos. In closing, we believe that a successful response has been made to the challenge issued at the XVIII General Assembly of the EGS.

Acknowledgments. Some support for A. A. Tsonis and G. N. Triantafyllou was provided by NSF Grant ATM-9310959, and for J. B. Elsner by NSF Grant ATM-9310715. Support for A. D. Kirwan Jr. and John J. Holdzkom II was provided by Grants N00014-91-J-1560 and N00014-93-1-0842 from ONR to Old Dominion University. A. D. Kirwan Jr. also acknowledges the Samuel L. and Fay M. Slover endowment to Old Dominion University.

References

Abarbanel, H. D. I., and M. B. Kennel, 1992: Local false nearest neighbors and dynamical dimensions from observed chaotic data. *Phys. Rev.*, **E47,** 3057–3068.

Ball, F. K., 1963: Some general theorems concerning the finite motion of a shallow rotating liquid lying on a paraboloid. *J. Fluid Mech.*, **19,** 240–256.

Cushman-Roisin, B., W. H. Heil, and D. Nof, 1985: Oscillations and rotations of elliptical warm-core rings. *J. Geophy. Res.*, **90**(C6), 11 756–11 764.

Eckmann, J. P., S. O. Kamphorst, D. Ruelle, and S. Ciliberto, 1986: Lyapunov exponents from time series. *Phys. Rev.*, **A34,** 4971–4980.

Elsner, J. B., and A. A. Tsonis, 1992: Nonlinear prediction, chaos and noise. *Bull. Amer. Meteor. Soc.*, **73,** 49–60.

Eringen, A. C., 1962: *Nonlinear Theory of Continuous Media.* McGraw-Hill, 477 pp.

Farmer, J. D., and J. J. Sidorowich, 1987: Predicting chaotic time series. *Phys. Rev. Lett.*, **59,** 845–848.

Gershenfeld, N. A., and A. S. Weigend, 1993: The future of time series: Learning and understanding. *Time Series Prediction: Forecasting the Future and Understanding the Past,* A. S. Weigend and N. A. Gerstienfeld, Eds., Addison–Wesley, 643 pp.

Grassberger, P., and I. Procaccia, 1983a: Characterization of strange attractors. *Phys. Rev. Lett.*, **50,** 346–349.

——, and ——, 1983b: Measuring the strangeness of strange attractors. *Physica,* **9D,** 189–208.

Kirwan, A. D., Jr., and J. Liu, 1991: Shallow water equations on an *f*-plane. *Nonlinear Topics in Ocean Physics,* A. R. Osborne, Ed., Course CIX, 99–132.

——, and B. L. Lipphardt Jr., 1993: Coherent flows with near zero potential vorticity. *J. Mar. Sys.*, **4**(2–3), 95–115.

——, ——, and J. Liu, 1992: Negative potential vorticity lenses. *Int. J. Eng. Sci.*, **30**(10), 1361–1378.

Ruddick, B. R., 1987: Anticyclonic lenses in large-scale strain and shear. *J. Phys. Oceanogr.*, **17,** 741–749.

Sugihara, G., and R. M. May, 1990: Nonlinear forecasting as a way of distinguishing chaos from measurement error in time series. *Nature,* **344,** 734–741.

Tsonis, A. A., 1992: *Chaos: From Theory to Applications.* Plenum, 274 pp.